

# 1 **High-resolution CTCF footprinting reveals impact of chromatin state on** 2 **cohesin extrusion dynamics**

3  
4 Corriene E. Sept<sup>1,2,3</sup>, Y. Esther Tak<sup>4,5</sup>, Christian G. Cerda-Smith<sup>6</sup>, Haley M. Hutchinson<sup>6</sup>, Viraat  
5 Goel<sup>3,7,8</sup>, Marco Blanchette<sup>9</sup>, Mital S. Bhakta<sup>9</sup>, Anders S. Hansen<sup>3,7,8</sup>, J. Keith Joung<sup>4,5</sup>, Sarah  
6 Johnstone<sup>3,10</sup>, Christine E. Eyler<sup>11,12</sup>, & Martin J. Aryee<sup>1,2,3</sup>

## 7 8 **Affiliations:**

9 <sup>1</sup>Department of Biostatistics, Harvard T.H. Chan School of Public Health; Boston, MA 02115,  
10 USA

11 <sup>2</sup>Department of Data Sciences, Dana-Farber Cancer Institute; Boston, MA 02115, USA

12 <sup>3</sup>Broad Institute of MIT and Harvard; Cambridge, MA 02142, USA

13 <sup>4</sup>Molecular Pathology Unit, Massachusetts General Hospital; Charlestown, MA 02129, USA

14 <sup>5</sup>Department of Pathology, Harvard Medical School; Boston, MA 02115, USA

15 <sup>6</sup>Department of Pharmacology and Cancer Biology, Duke University School of Medicine;  
16 Durham, NC 27710, USA.

17 <sup>7</sup>Department of Biological Engineering, Massachusetts Institute of Technology; Cambridge, MA  
18 02139, USA

19 <sup>8</sup>Koch Institute for Integrative Cancer Research; Cambridge, MA 02139, USA

20 <sup>9</sup>Dovetail Genomics, Cantata Bio LLC, Scotts Valley, CA 95066, USA

21 <sup>10</sup>Department of Pathology, Dana-Farber Cancer Institute; Boston, MA 02215, USA.

22 <sup>11</sup>Department of Radiation Oncology, Duke University School of Medicine; Durham, NC 27710,  
23 USA.

24 <sup>12</sup>Duke Cancer Institute, Duke University School of Medicine; Durham, NC 27710, USA.

## 25 26 27 **Abstract**

28  
29 DNA looping is vital for establishing many enhancer-promoter interactions. While CTCF is  
30 known to anchor many cohesin-mediated loops, the looped chromatin fiber appears to  
31 predominantly exist in a poorly characterized actively extruding state. To better characterize  
32 extruding chromatin loop structures, we used CTCF MNase HiChIP data to determine both  
33 CTCF binding at high resolution and 3D contact information. Here we present *FactorFinder*, a  
34 tool that identifies CTCF binding sites at near base-pair resolution. We leverage this substantial  
35 advance in resolution to determine that the fully extruded (CTCF-CTCF) state is rare genome-  
36 wide with locus-specific variation from ~1-10%. We further investigate the impact of chromatin  
37 state on loop extrusion dynamics, and find that active enhancers and RNA Pol II impede cohesin  
38 extrusion, facilitating an enrichment of enhancer-promoter contacts in the partially extruded loop  
39 state. We propose a model of topological regulation whereby the transient, partially extruded  
40 states play active roles in transcription.

## 41 **Background**

42  
43 Topologically associated domains (TADs) and regulatory enhancer-promoter chromatin loops  
44 are largely formed by the cohesin complex through the process of CTCF-mediated loop  
45 extrusion<sup>1,2</sup>. Topological alterations and subsequent changes in enhancer-promoter (EP) contacts  
46 can modify gene expression<sup>3,4</sup> and cause aberrant phenotypes<sup>5-8</sup>. CCCTC-binding factor (CTCF)  
47 can act as an extrusion barrier through its ability to bind and stabilize cohesin on DNA, serving  
48 to preferentially localize and anchor one or both ends of cohesin loops. Genes with promoter-  
49 proximal CTCF binding sites have been shown to have increased dependence on distal  
50 enhancers<sup>9-11</sup>, although the exact mechanisms involved are not well understood.

51  
52 Although conventional 3C techniques give an impression of static loops, cohesin-mediated  
53 chromatin loops are actually dynamic with an extrusion rate of ~1kb/s<sup>12</sup>. Recent live cell-  
54 imaging studies of two TADs found that the fully extruded state with a loop formed between two  
55 convergent CTCF-bound anchors was present only 3-30% of the time<sup>13,14</sup>. While these findings  
56 suggest that CTCF loops spend the vast majority of their time partially-extruded, the partially-  
57 extruded state has not yet been well characterized.

58  
59 Several studies have found evidence of promoter-proximal CTCF binding sites (CBS) having  
60 large impacts on EP contact frequencies and transcription<sup>9-11</sup>. Putting this together with the high  
61 prevalence of partially extruded CTCF-mediated loops, we hypothesize that promoter-proximal  
62 CTCF sites enable gene regulation by halting cohesin on one side while cohesin continues to  
63 extrude on the other side. Enhancers then slow down extrusion, thus enabling an increase in EP  
64 contacts without requiring a fully extruded loop. The relationship between EP contacts and  
65 transcription can be nonlinear such that small increases in EP contacts may cause large changes  
66 in transcription<sup>3,4</sup>. As a result, even minor decreases in extrusion rate through enhancer regions  
67 may affect gene expression.

68  
69 The ability of MNase to efficiently digest naked DNA while sparing protein-bound DNA has  
70 been employed in various strategies to footprint the binding sites of proteins such as transcription  
71 factors with near base-pair resolution<sup>15-18</sup>. A key advantage of using MNase over sonication-  
72 based protocols is the shorter fragment size obtained, which directly leads to higher resolution  
73 TF binding site identification. More recently, MNase DNA fragmentation has also been applied  
74 to proximity ligation assays to map 3D genome architecture with nucleosome (~150 bp)  
75 resolution, enabling precise characterization of 3D architecture including at TAD boundaries and  
76 punctate enhancer-promoter interactions<sup>19-22</sup>. Since MNase HiChIP enables precise  
77 characterization of both TF-binding and 3D contacts, it is uniquely poised to define how CTCF  
78 enables 3D contacts.

79

80 To better characterize the partially extruded chromatin loop state, we first develop a  
81 computational technique for high-resolution footprinting of CTCF using MNase HiChIP data.  
82 We then employ this to study how, through its interaction with the looping factor cohesin, CTCF  
83 can facilitate long-range DNA contacts. We further characterize how the length of loops  
84 extruded by cohesin is affected by local chromatin state factors such as enhancer and RNA Pol II  
85 density.

86

## 87 **Results**

88

### 89 *MNase HiChIP generates short, TF-protected and longer, histone-protected DNA* 90 *fragments*

91 We used Micrococcal nuclease (MNase) HiChIP<sup>23</sup> with a CTCF antibody to profile 3D  
92 architecture in K562 cells, generating 150 bp reads with over 380 million unique pairwise  
93 contacts across four replicates. Briefly, following cell fixation with DSG and formaldehyde,  
94 chromatin is digested by MNase, immunoprecipitated to enrich for CTCF-bound DNA, and free  
95 ends are then ligated. After reverse-crosslinking, the resulting ligation products are sequenced  
96 from both ends and the mapping locations of the paired reads can be used to infer chromosomal  
97 locations of the physically interacting loci. In cases where the pre-ligation fragments are shorter  
98 than the read length it is also possible to infer the fragment length as the ligation junction  
99 position will be observed within one or both of the reads. If multiple fragments within a read are  
100 short enough to be aligned to distinct genomic locations, this is termed an ‘observed ligation’  
101 (Fig. 1a, Supp Fig 1).

102

103 As expected, due to the preference of MNase to selectively cleave DNA not shielded by bound  
104 proteins and the high abundance of histones in chromatin (Fig. 1b), the predominant fragment  
105 length is approximately 150 bp, indicative of cuts between nucleosomes<sup>24</sup> (Fig 1c). We also  
106 noted a distribution of shorter fragment lengths, with 20% representing lengths shorter than 120  
107 bp (Fig. 1d). A metaplot centered on CTCF binding site motifs shows an enrichment of 30-60 bp  
108 fragments suggesting that these shorter fragments represent CTCF-bound DNA (Fig. 1c)<sup>2,25,26</sup>.  
109 Consistent with this, we find that short (<80 bp) fragments have a 10-fold higher overlap  
110 frequency with CTCF motifs than long (>120 bp) fragments (Fig. 1d). This is similar to data  
111 from the MNase-based CUT&RUN assay that also results in short fragments protected by small  
112 proteins such as transcription factors<sup>17</sup>.

113

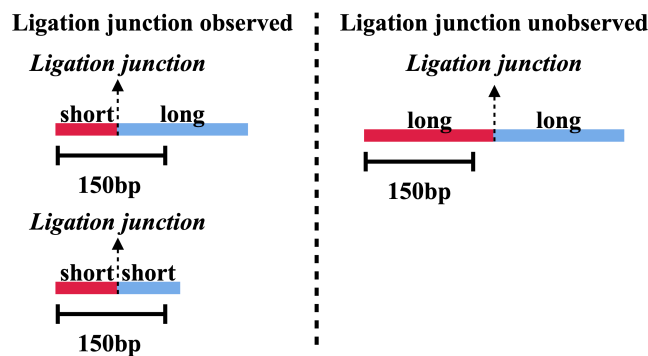
114 Fragment pileups at CTCF motif loci (Fig. 1e) show a strong enrichment of short fragments  
115 centered on the CTCF motif sequence, and a concomitant depletion of long fragments at motifs  
116 (Fig. 1f). Long fragments, in contrast, show peaks with a strong ~200 bp periodicity adjacent to  
117 the central CTCF binding site (Fig. 1f). This is consistent with the ability of CTCF to precisely  
118 position a series of nucleosomes adjacent to its binding site<sup>25</sup>. Note that while long (>120 bp)  
119 fragments are depleted at CTCF binding sites, they still represent a significant fraction of reads at

120 these sites (Fig. 1c). This likely reflects that CTCF motif loci without a bound CTCF are  
 121 frequently instead occupied by histones<sup>25</sup>, and even CTCF motifs with very strong CTCF ChIP-  
 122 seq signal are not always occupied by a CTCF.

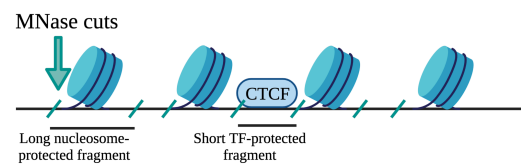
123

124 In summary, long fragments correspond to nucleosome-protected DNA whereas short fragments  
 125 arise from TF-protected DNA. This is due to the different sizes of CTCF and histone octamers,  
 126 with nucleosomes protecting about twice the amount of DNA that CTCF protects<sup>25</sup>. Since  
 127 MNase cuts around bound proteins, the different protein sizes directly translate to different  
 128 fragment lengths. Accordingly, we next filter out long, nucleosome-protected fragments and  
 129 focus on short, TF-protected fragments to identify CBS.

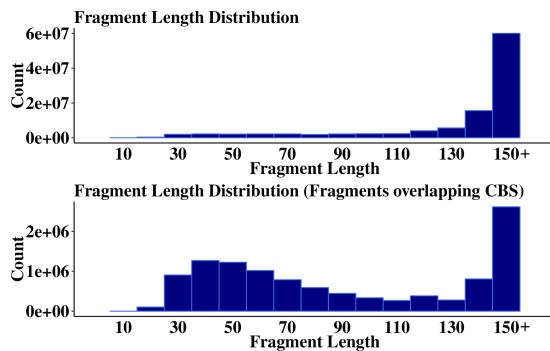
**a**



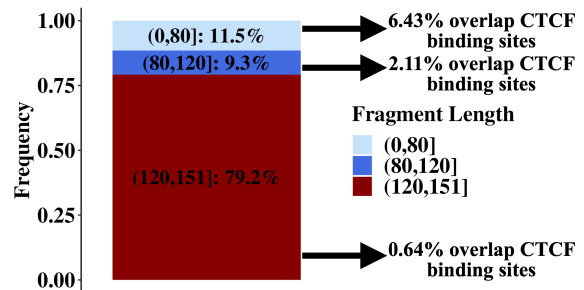
**b**



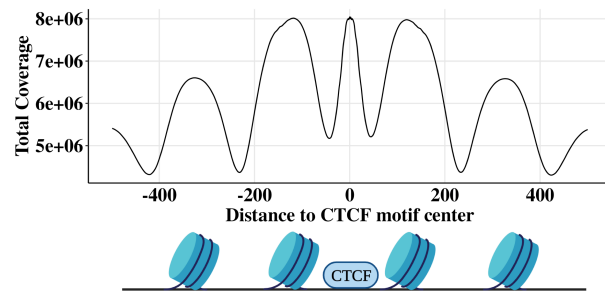
**c**



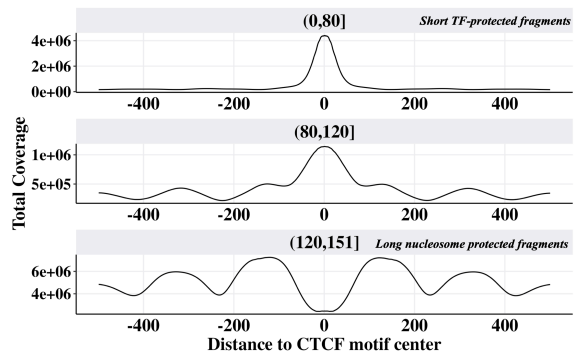
**d**



**e**



**f**



130



131 **Fig. 1** MNase CTCF HiChIP data contains short ( $\sim <80$  bp) CTCF-protected fragments and  
132 longer ( $\sim >120$  bp) nucleosome-protected fragments. **a** Schematic illustrating relationship  
133 between short fragments and observed ligations. **b** Schematic illustrating how the fragment  
134 length results from MNase cutting around bound proteins of different sizes. **c** Fragment length  
135 distribution for all fragments (top plot) and fragments overlapping occupied CTCF motifs (lower  
136 plot). Occupied CTCF motifs are defined here as CTCF motifs within 30 bp of a CTCF ChIP-seq  
137 peak summit. **d** Boxplot quantifying the frequency of different fragment lengths genome-wide  
138 and how often each fragment length group overlaps an occupied CTCF motif. Occupied CTCF  
139 motifs are defined here as CTCF motifs within 30 bp of a CTCF ChIP-seq peak summit. **e**  
140 Fragment coverage metaplot  $\pm 500$  bp around CTCF binding sites. Schematic below the  
141 coverage metaplot illustrates the proteins producing these peaks. **f** Plot **(e)** stratified by fragment  
142 length.

143

144 *FactorFinder leverages the strand-specific bimodal distribution of short fragments*  
145 *around CBS to obtain precise detection of CTCF binding*

146 In order to characterize CTCF-mediated chromatin loop interactions, we first set out to map  
147 CTCF loop anchors with high resolution. We take advantage of the difference in fragment  
148 lengths associated with CTCF-bound vs nucleosome-bound DNA to focus only on likely CTCF-  
149 bound fragments. Fragment lengths can be determined for all fragments with length less than 150  
150 bp; the 150 bp read length results in censoring of fragments longer than 150 bp. While exact  
151 fragment lengths can be obtained for all fragments shorter than 150 bp, observed ligations  
152 require a shorter fragment length. This is because observed ligations require distinct mapping of  
153 fragments on either side of the ligation junction. Since at least  $\sim 25$  bp are required to align a  
154 sequence to the reference genome, this results in fragments characterized as observed ligations  
155 having a maximum fragment length of  $\sim 125$  bp, sufficient for the identification of most CTCF-  
156 protected DNA fragments. Consequently, the fraction of informative, CTCF-protected fragments  
157 decreases with shorter sequencing read length (Supp Fig 1). The effect of subsetting the CTCF  
158 HiChIP dataset to only short fragments ( $<125$  bp, identified by the proxy of an observed  
159 ligation), is shown in Fig 2a,b. These shorter, presumably CTCF-protected fragments, are  
160 overwhelmingly located immediately adjacent to CTCF motifs.

161

162 Sequencing of short, CTCF-protected fragments results in a bimodal read distribution centered  
163 on the CBS, with read 5' location peaks observed upstream (positive strand) and downstream  
164 (negative strand) of the CBS (Fig. 2c). We refer to these regions as quadrants 2 and 4 (Q2 and  
165 Q4) respectively (Fig. 2d, e). In contrast, reads from the positive strand downstream of the CBS  
166 (Q1) and negative strand upstream of the CBS (Q3) correspond to fragments with MNase cut  
167 sites underneath CTCF-protected DNA, and therefore reflect a lack of CTCF occupancy. CTCF  
168 binding therefore produces an enrichment of reads in Q2,Q4 and a depletion of reads in Q1,Q3  
169 (Fig. 2e). At sites without protein binding, MNase can cut at any location resulting in no  
170 enrichment of reads in Q2 and Q4 compared to Q1 and Q3 (Fig. 2e). As a result, we can

171 determine CTCF binding by testing if there are significantly more reads in Q2 and Q4 than Q1  
172 and Q3 (Fig. 2f).

173

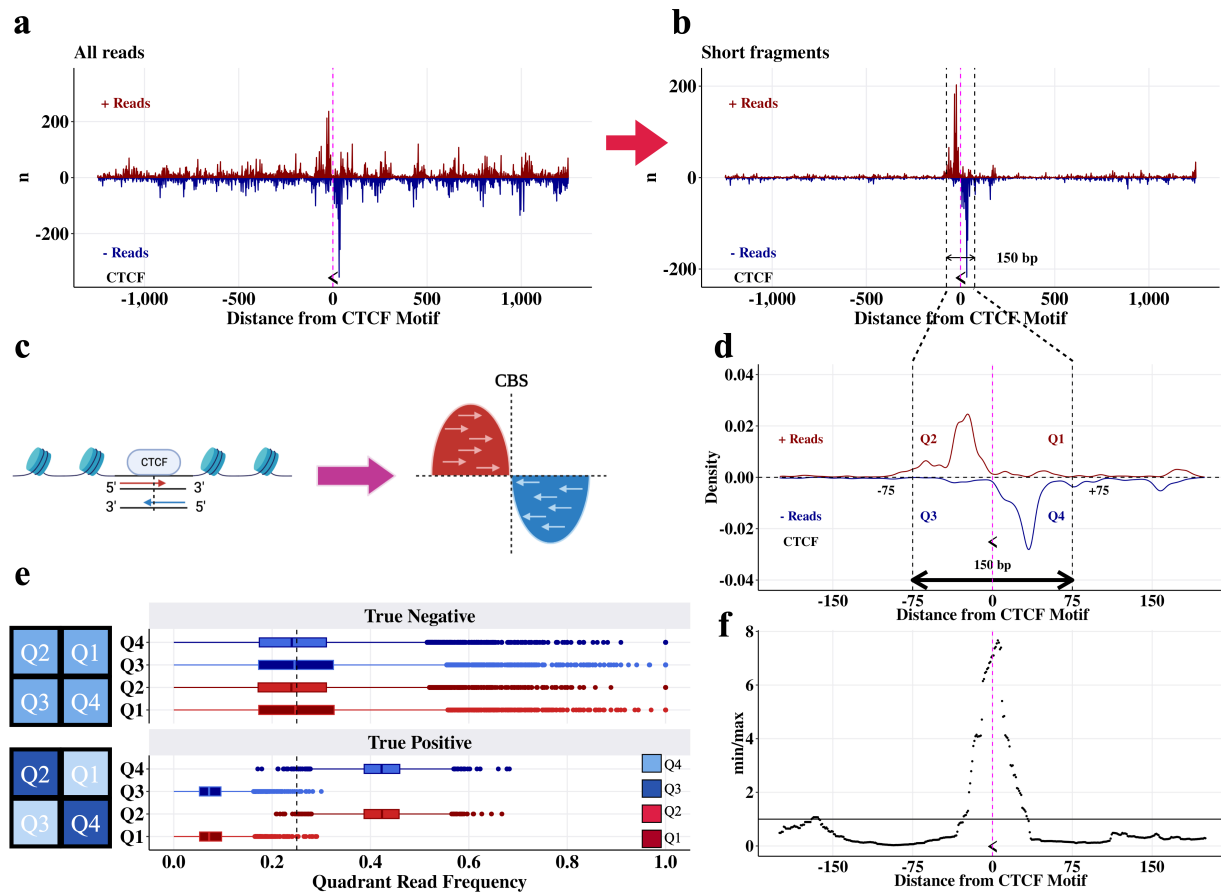
174 We can consider each read as an independent draw from a multinomial distribution with four  
175 categories corresponding to the four quadrants. Under the null hypothesis, each read has equal  
176 probability of belonging to any of the four quadrants  $Q_i, i \in \{1,2,3,4\}$ . Because true CTCF  
177 binding induces a strong read pile-up in *both* quadrants 2 and 4 in addition to a depletion of reads  
178 in quadrants 1 and 3 (Fig. 2d, e, f), we test for an enrichment of reads in Q2 and Q4 compared to  
179 Q1 and Q3 by estimating the *FactorFinder* statistic  $\hat{\alpha} = \frac{\min(n_2, n_4)}{\max(n_1, n_3)}$ , where  $n_i$  is the number of  
180 reads in  $Q_i$ . We then test if  $\hat{\alpha}$  is significantly greater than 1. Note that min and max are used to  
181 enforce that both quadrants 2 and 4 must have more reads than both quadrants 1 and 3; using the  
182 average would enable read pile-ups that occur in quadrant 2 or 4 (but not both) to be spuriously  
183 called as CTCF binding events.

184

185 To evaluate the significance of  $\hat{\alpha}$  at a particular total read count  $N = \sum_{i=1}^4 n_i$ , we simulated 100  
186 million samples under the null hypothesis that each fragment is equally likely to occur in any of  
187 the four quadrants. This was done at each total read count ranging from 5 to 500. P-values at read  
188 counts beyond 500 are very similar to those at 500, so 500+ read counts are treated as bins with  
189 500 total read count (Supp Fig 2). The empirical CDF of the 100 million  $\log_2(\hat{\alpha})$  at a given total  
190 read count was then computed and used to evaluate the probability of observing a value more  
191 extreme than  $\log_2(\hat{\alpha})$  under the null hypothesis. The empirical CDF was evaluated at a sequence  
192 of possible  $\log_2(\hat{\alpha})$  between 0 and 5 at step sizes of 0.01 (this corresponds to  $\hat{\alpha} \in [1, 32]$ .) This  
193 approach produces the same p-values as using  $\hat{\alpha}$  instead of  $\log_2(\hat{\alpha})$ , but using the log enables  
194 smaller step size at large values of  $\hat{\alpha}$ . After acquiring the grid of p-values for each  $\hat{\alpha}$  at a given  
195 read count  $N$ , we match the observed  $\hat{\alpha}$  at a read count of  $N$  with the corresponding p-value from  
196 the table. Because this approach only requires quadrant-specific read counts to match with the  
197 given table of p-values, it is very computationally efficient. Furthermore, by using the  
198 multinomial framework we place no assumptions on the reads within each quadrant being  
199 distributed as poisson, negative binomial, or another distribution. The only assumption we make  
200 is that in the event of no CTCF binding, the reads are equally distributed amongst the four  
201 quadrants. We have shown this assumption holds in Figures 2c, d, e.

202

203 In brief, we have shown that short fragments exhibit a strand-specific, bimodal distribution  
204 centered on the CBS. This distribution arises from MNase cutting around a bound CTCF and  
205 subsequent sequencing 5' to 3' of the DNA. Significance is assessed through a multinomial  
206 framework, which has the advantage of not placing any assumptions on the distribution of reads  
207 within each quadrant. Now that we have explored the theory behind *FactorFinder*, we  
208 demonstrate its ability to identify CBS with high resolution and accuracy.



209  
 210 **Fig. 2** True CTCF binding sites have a bimodal strand-specific distribution centered on the  
 211 CTCF motif. **a** Unfiltered reads +/- 1250 bp around a CTCF binding site located on the negative  
 212 strand (chr1: 30,779,763 - 30,779,781). The midpoint of the CTCF motif is marked with the  
 213 symbol “<”, representing that it is on the negative strand, and a pink line. **b** Plot **(a)** filtered to  
 214 observed ligations (equivalently, short fragments.) **c** Schematic demonstrating the bimodal read  
 215 pile-up around a CTCF binding site. **d** Plot **(b)** as a density plot and zoomed in on the CTCF  
 216 motif, with quadrant annotations. **e** Distributions of reads in quadrants for true negative and true  
 217 positive CTCF binding sites in DNA loop anchors. True positives are defined as CTCF motifs  
 218 that are the only CTCF motif in a loop anchor and within 30 bp of a CTCF ChIP-seq peak. True  
 219 negatives are areas of the loop anchors with one CTCF motif that are at least 200 bp from the  
 220 CTCF motif. Schematics of the quadrant read pile-up patterns are shown next to the  
 221 corresponding true positive and true negative boxplots. **f** *FactorFinder* statistic ( $\hat{\alpha} = \frac{\min(n_2, n_4)}{\max(n_1, n_3)}$ )  
 222 for plot **(d)** peaks at the CTCF motif.  
 223

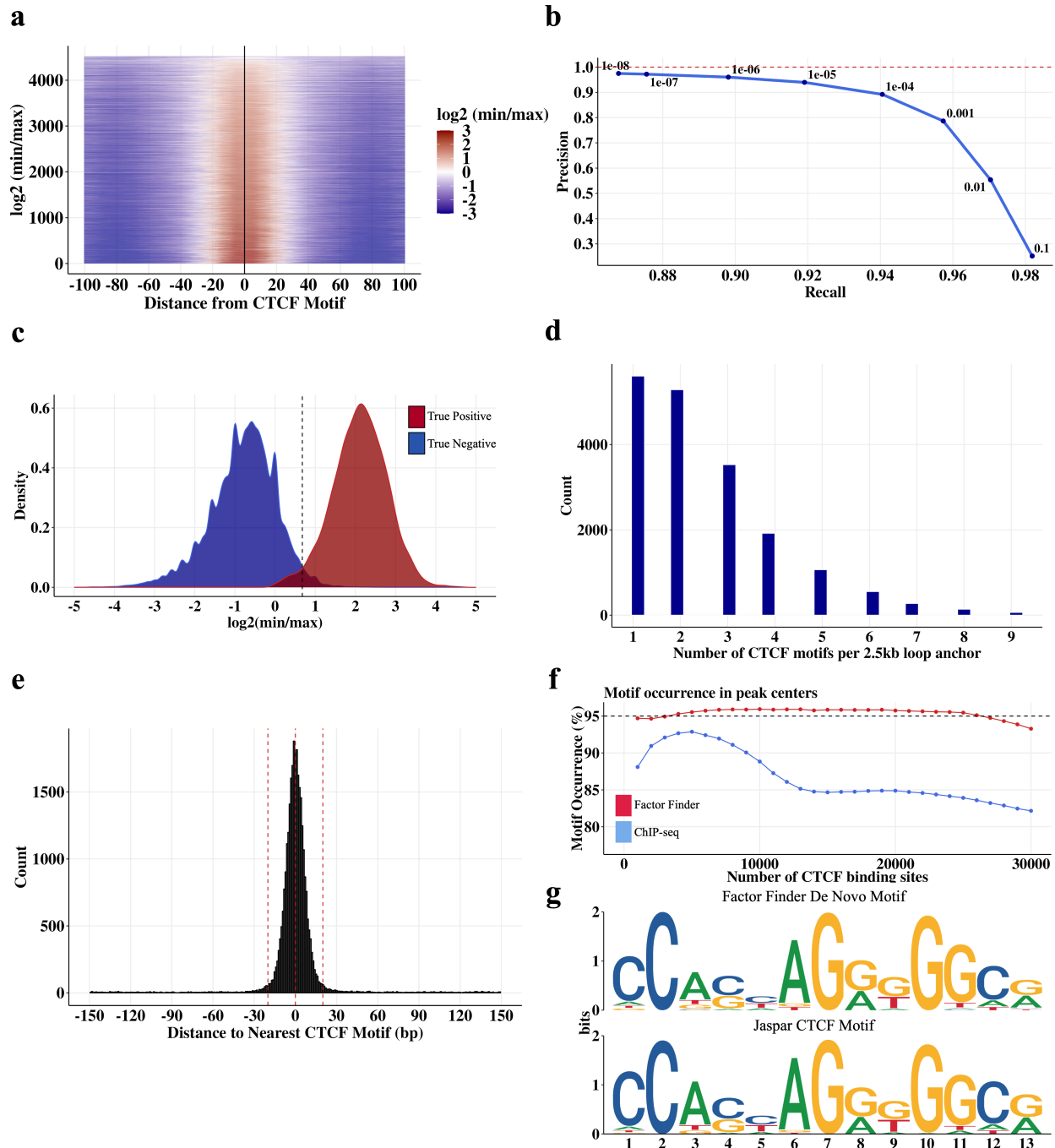
## 224 Model evaluation

225 *FactorFinder* uses a biologically-informed model that takes advantage of the distribution of short  
 226 fragments around a CTCF binding site to pinpoint CTCF binding. Additionally, our use of a  
 227 multinomial framework for significance evaluation avoids placing any distributional assumptions

228 on the reads within a quadrant. We then sought to benchmark our CTCF binding site  
229 identification performance using CTCF motif locations<sup>27</sup>, CTCF ChIP-seq peaks<sup>28</sup>, and loop  
230 anchors identified by FitHiChIP at 2.5kb resolution<sup>29</sup>.

231  
232 We define a high stringency true positive set of CTCF binding sites as CTCF motifs in loop  
233 anchors that are located within 30 bp of a CTCF ChIP-seq peak summit. To avoid ambiguity due  
234 to multiple closely spaced motifs, we further selected only those motifs that are unique within a  
235 2.5kb loop anchor. Using this true positive set, we observe that the *FactorFinder* statistic,  
236  $\log_2(\hat{\alpha}) = \log_2\left(\frac{\min(n_2, n_4)}{\max(n_1, n_3)}\right)$  has signal greater than 0 (equivalently,  $\hat{\alpha} > 1$ ) almost exclusively  
237 within 20 bp of the CTCF motif center and centered on 0 bp from the CTCF motif center (Fig.  
238 3a). Using this same set of true positive sites (false negatives are the regions of the loop anchors  
239 >200 bp from a CTCF motif), we achieve > 90% precision and > 90% recall at a p-value  
240 threshold of 1e-05, and maintain high recall and precision at all p-value thresholds < 1e-05 (Fig.  
241 3b). This high level of recall and precision is achieved because of the very different  
242 *FactorFinder* statistic distributions for true positives and true negatives (Fig. 3c).

243  
244 Because 70% of loop anchors defined with 2500 bp resolution contain multiple CTCF motifs  
245 (Fig. 3d), higher levels of precision are often needed to determine the specific CTCF motif(s)  
246 mediating a CTCF loop. Examining the effectiveness of *FactorFinder* genome-wide, we observe  
247 that almost all *FactorFinder* peak summits (93%) are within 20 bp of a CTCF motif center, with  
248 a median separation of 5 bp (Fig. 3e). Quantifying accuracy using motif occurrence within 20 bp  
249 of a peak summit, we find that *FactorFinder* maintains ~95% motif occurrence while ChIP-seq  
250 declines to less than 85% motif occurrence (Fig. 3f). Applying the motif discovery tool  
251 STREME<sup>30</sup> to 30 bp sequences centered on the *FactorFinder* peak summit produces a motif  
252 sequence that exactly matches the core JASPAR CTCF motif (Fig. 3g), further supporting  
253 *FactorFinder*'s ability to identify true CTCF binding sites.



254  
 255 **Fig. 3** CTCF binding sites identified by *FactorFinder* with single basepair resolution in MNase  
 256 K562 CTCF HiChIP data. **a** Heatmap of  $\log_2(\min/\max)$  as a function of distance between  
 257 *FactorFinder* peak center and CTCF motif center within loop anchors. Only CTCF motifs that  
 258 are unique within a loop anchor and within 30 bp of a CTCF ChIP-seq peak are used. **b** Precision  
 259 recall curve for true negative and true positive CTCF binding sites in DNA loop anchors. True  
 260 positives are defined as in **(a)**. True negatives are areas of the loop anchors in **(a)** that are at least  
 261 200 bp from the one CTCF motif. Precision is calculated as  $TP / (TP + FP)$ , recall is calculated

262 as  $TP / (TP + FN)$ . **c** *FactorFinder* statistic density plots using the same set of true positives and  
263 true negatives as **(b)**. **d** Distribution of the number of CTCF motifs in a 2.5kb loop anchor. **e**  
264 Histogram with 1 bp bin size depicting *FactorFinder* resolution for all peaks genome-wide (not  
265 just in loop anchors). **f** Motif occurrence in ChIP-seq and *FactorFinder* peak centers genome-  
266 wide. Motif occurrence is calculated as % peak centers within 20 bp of CTCF motif. Only peak  
267 centers within 150 bp of a CTCF motif are used for this figure. **g** 30 bp sequences centered on  
268 genome-wide *FactorFinder* peak centers produce a de novo motif (top) that matches the core  
269 JASPAR CTCF motif (bottom).

270

### 271 *CTCF and Cohesin occupancy footprints*

272 We next examined the length characteristics of MNase HiChIP fragments overlapping individual  
273 CTCF motifs, to infer the presence and identity of the protein occupying the locus. For motifs  
274 with non-zero coverage, we observed long, 150+ bp fragments, as shown for three representative  
275 motifs in Figure 4a. These fragments likely represent cells with a nucleosome located at the  
276 motif locus, and are observed at CTCF motifs genome-wide (Fig. 1c). In addition, for a large  
277 subset of CTCF motifs, we also observed short, sub-nucleosome sized (<115 bp) fragments (Fig.  
278 4a, Fig. 1c), likely instead representing DNA protected by CTCF.

279

280 A closer examination of the TF-scale fragments at *FactorFinder*-identified bound motifs reveals  
281 that they tend to exhibit a skew towards the downstream side of the CTCF motif (Fig. 4a, b, c),  
282 suggesting a preferred location for the protein(s) protecting the region from MNase cleavage. We  
283 considered cohesin as a potential candidate, given a recent finding that cohesin is stabilized on  
284 DNA through a specific interaction with the N terminus of the CTCF protein<sup>2</sup>, which localizes to  
285 the downstream side of the CTCF binding site.

286

287 Given CTCF's role in mediating DNA looping we investigated whether the CTCF-adjacent  
288 protected footprint might relate to 3D architecture within the cell. We used HiChIP pairwise  
289 interaction data where each ligation event reflects a single-cell point-to-point contact, to classify  
290 each CTCF motif-overlapping fragment as either 'upstream' or 'downstream', depending on its  
291 relationship to its interaction partner. Upstream fragments have long range contacts downstream  
292 of the motif, and therefore have looping contacts in the same direction as a chromatin loop  
293 mediated by cohesin bound to the N terminus of the CTCF protein. Examining the difference in  
294 coverage downstream and upstream of CBS genome-wide, we observe that upstream fragments  
295 overlapping CBS with an adjacent strong RAD21 ChIP-seq peak have substantially more  
296 adjacent coverage in the ~60 bp region downstream compared to upstream of the motif, while  
297 downstream fragments and CBS with weak adjacent RAD21 ChIP-seq peaks exhibit no  
298 difference (Fig. 4d). This finding further suggests that the CTCF-adjacent factor is associated  
299 with loop formation.

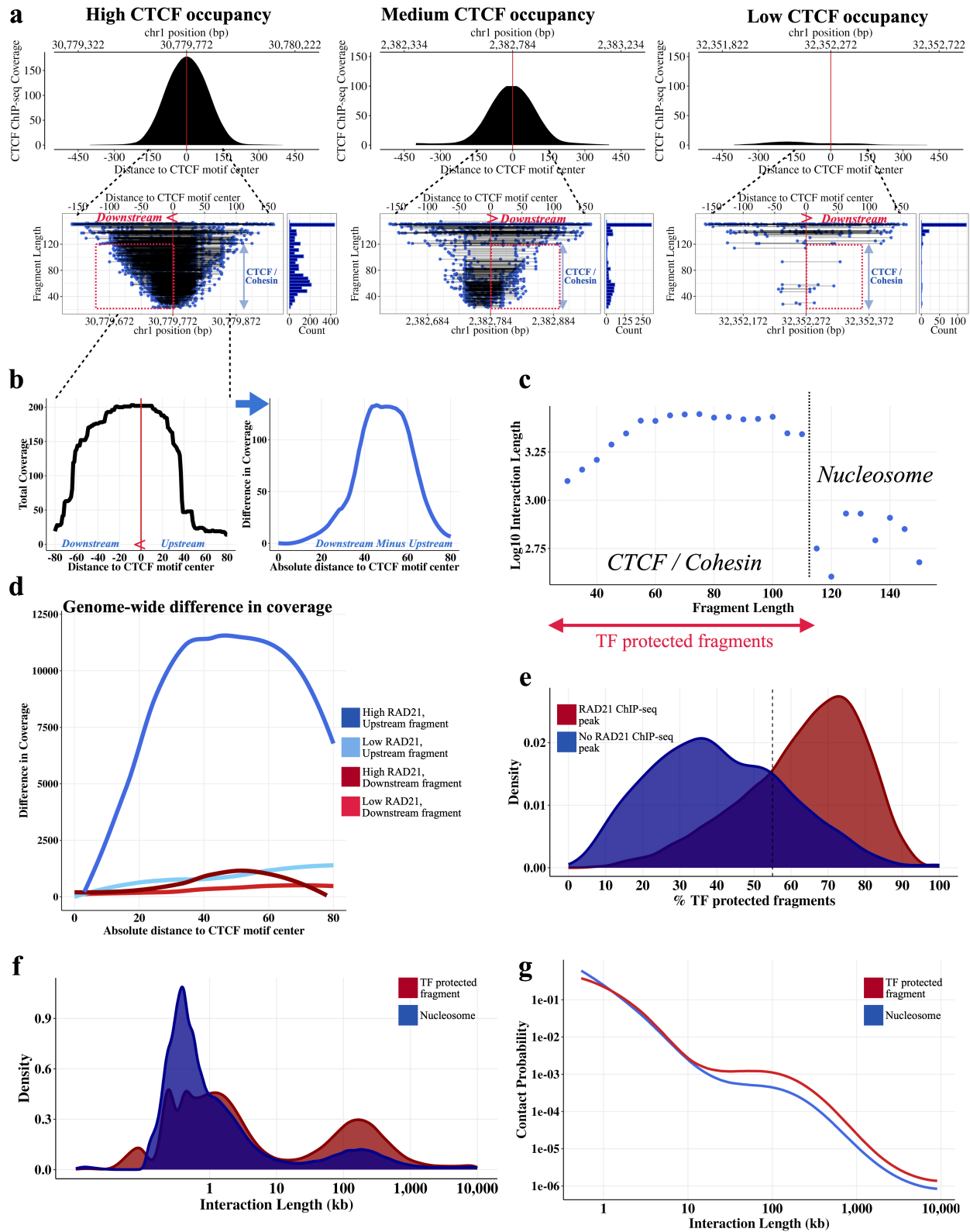
300



301 To further investigate whether the TF footprints identified at CTCF motifs might relate to an  
302 architectural role, we used HiChIP data to characterize their interaction patterns. We found that  
303 TF-protected fragments (<115 bp) had contacts at substantially longer genomic distances than  
304 nucleosome-protected fragments (Fig. 4c), suggesting that the TF presence may facilitate long  
305 range interactions. Furthermore, we computed the frequency of TF-protected fragments at all  
306 *FactorFinder*-identified CTCF bound sites, and found that it is strongly associated with the  
307 presence of a RAD21 ChIP-Seq peak at the motif<sup>28</sup> (Fig 4e).

308

309 Examination of the interaction length distribution shows that, as expected, the majority of  
310 interactions occur within a linear separation of less than 10kb. The fraction of long-range  
311 (>10kb) interactions, however, is significantly enriched (3.5-fold,  $p < 10^{-10}$ ) for short TF-  
312 protected fragments as would be expected if these footprints represent CTCF/cohesin (Fig. 4f).  
313 Similarly, an examination of the P(s) curve, showing contact probability as a function of linear  
314 distance, reveals a decreased attenuation in contact probability at longer interaction lengths (Fig.  
315 4g). Taken together, these findings suggest that we can classify CTCF HiChIP interaction data  
316 based on footprint/fragment size as involving either unoccupied CTCF sites that tend to have  
317 short-range chromatin interactions, or CTCF/cohesin occupied sites that, presumably through  
318 loop extrusion, are able to make long-range contacts.



319  
320  
321

**Fig. 4** Cohesin and CTCF-protected fragments identified in CTCF MNase HiChIP. **a** High, medium, and low CTCF occupied motifs. Cohesin footprint is observed downstream of the CBS

322 for high and medium CTCF occupancy motifs. For each occupancy level, CTCF ChIP-seq (top)  
323 and all fragments overlapping the CTCF motif (bottom left) are depicted, along with the  
324 corresponding fragment length histogram (bottom right). **b** Locus-specific high CTCF occupancy  
325 figure from **(a)** as a coverage plot (left figure), difference in coverage between downstream and  
326 upstream coverage (right figure). **c** Plotting median log<sub>10</sub> interaction length as a function of  
327 fragment length suggests presence of nucleosome vs TF-protected fragments. Only left  
328 fragments overlapping CTCF (+) motifs with start and end at least 15 bp from the CTCF motif  
329 were included in this graph to remove confounding by MNase cut site. Using this figure, we are  
330 approximating CTCF +/- cohesin-protected fragments as those with fragment length < 115, start  
331 and end at least 15 bp from the motif center. **d** Difference in coverage (downstream - upstream)  
332 across all CBS shows an increase in coverage downstream of the CTCF motif for upstream  
333 fragments underlying CBS with a strong adjacent RAD21 ChIP-seq peak. **e** CTCF motifs that  
334 have a nearby RAD21 ChIP-seq peak (within 50 bp) have a larger proportion of TF-protected  
335 fragments. **f** TF-protected fragments have a noticeably larger bump in density of long range  
336 interactions compared to nucleosome-protected fragments. Fragments were first filtered to those  
337 with start and end at least 15 bp from the motif. TF-protected fragments were then defined as  
338 fragments with length < 115 bp while nucleosome-protected fragments are fragments with length  
339 at least 115 bp. **g** P(S) curve for fragments depicted in **(f)**.

340

#### 341 Active enhancers and gene transcription hinder cohesin-mediated loop extrusion

342 Using the techniques described above, MNase HiChIP enables us to simultaneously locate CBS  
343 at high resolution, identify footprints of bound proteins, and interrogate specific chromatin  
344 contacts at the single molecule level. We next sought to leverage these data to characterize  
345 cohesin extrusion dynamics in a range of genomic contexts.

346

347 We first estimated the frequency of fully extruded CTCF-CTCF chromatin loops genome-wide.  
348 By obtaining fragments overlapping CTCF binding sites and estimating the fraction of  
349 interaction partners overlapping a downstream convergent CTCF motif, we obtain 5% as the  
350 genome-wide frequency of the fully extruded CTCF-CTCF state. We also find a wide CBS to  
351 CBS variability with an estimated range of ~1-10% (Fig. 5a). This suggests that most CTCF-  
352 anchored chromatin contacts at the single-cell level are in the ‘extruding’ state, rather than  
353 joining two CTCF sites. These ranges are consistent with two recent locus-specific live cell  
354 imaging studies, which found that the fully extruded loop state is rare at the *Fbn2* TAD<sup>13</sup> and an  
355 engineered TAD on chr15<sup>14</sup>, occurring ~3-6%<sup>13</sup> and ~20-30% of the time<sup>14</sup> respectively. Note  
356 that the 20-30% estimate corresponds to a loop existing between any combination of three CBS  
357 (+) and three CBS (-).

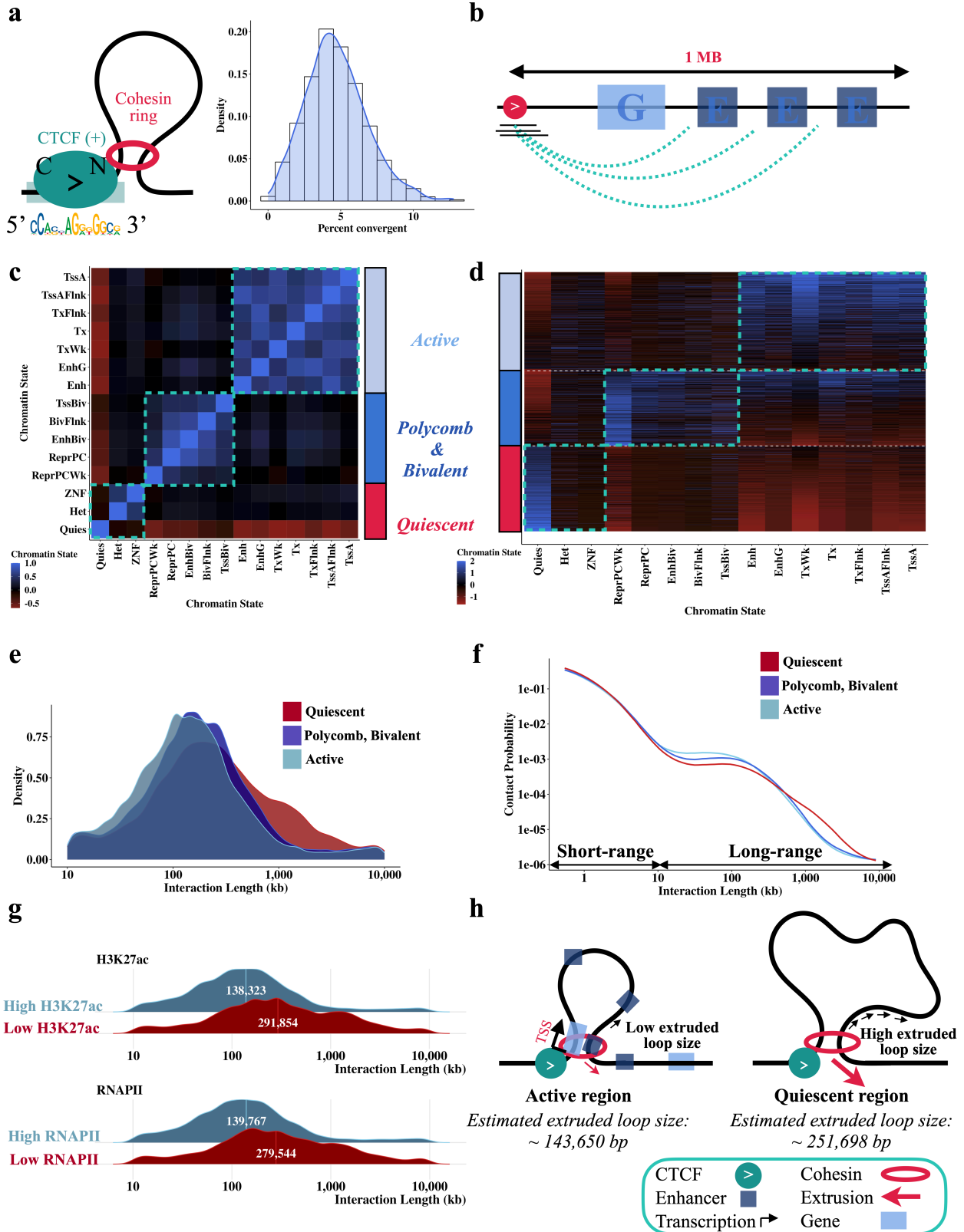
358

359 We next sought to use our data to examine how cohesin extrusion is impacted by chromatin  
360 context. Since HiChIP libraries are a snapshot of millions of cells, we can estimate dynamic  
361 extrusion parameters (primarily the average loop size extruded by cohesin<sup>31</sup>) from the interaction

362 length distribution. To determine the impact of chromatin state on cohesin extrusion, we first  
363 annotated the 1 MB regions downstream of *FactorFinder* identified CBS with ChromHMM  
364 states<sup>32</sup> (Fig. 5b) to characterize the DNA through which a cohesin anchored at the CBS would  
365 extrude through. Due to the highly correlated nature of ChromHMM annotations (Fig. 5c, d), we  
366 then divided the genome into three main chromatin state categories to uniquely classify each 1  
367 MB region as either active, polycomb/bivalent or quiescent (Fig. 5d). CTCF/cohesin-protected  
368 fragments overlapping CBS were accordingly annotated with the corresponding motif-level  
369 chromatin state group, and extruded loop size estimates were obtained for each chromatin state  
370 based on the fragment-level interaction lengths.

371  
372 Interestingly, we find that cohesin extrudes 1.75 times further through quiescent regions (252kb)  
373 than through active regions (144kb), corresponding to a difference in average extruded loop size  
374 of ~110kb,  $p < 10^{-10}$  (Fig. 5e, Supp Fig. 3, Supp Fig. 4 right). The P(s) curve, a plot of interaction  
375 decay with distance, confirms a depletion of the longest-range interactions in active regions (Fig  
376 5f). This estimate for quiescent regions is consistent with a live cell imaging study of the *Fbn2*  
377 locus in the absence of transcription that estimated a processivity of 300kb<sup>13</sup>. As quiescent  
378 regions are characterized by low TF binding, low transcription, and minimal histone  
379 modifications<sup>33</sup>, we hypothesized that the substantial difference in extruded loop size relates to  
380 gene activity and enhancer density obstructing loop extrusion. Consistent with this, we found  
381 that higher levels of H3K27ac and RNA Pol II binding in the 1MB region downstream of the  
382 CBS strongly correlate with lower average extruded loop size (Fig. 5g).

383  
384 We sought to establish that the observed differences in loop extrusion length as a function of  
385 chromatin state are not confounded by locus-specific effects on cohesin extrusion. Each CBS has  
386 locus-specific genetic architecture and a different number of overlapping fragments, so we fit a  
387 linear mixed effects model to account for this group-level heterogeneity. Specifically, we  
388 compute the ‘cohesin effect’ on loop length, defined as the increase in average interaction length  
389 for CTCF/cohesin bound fragments compared to nucleosome bound fragments for each CBS.  
390 Controlling for the background interaction frequency of a region in this way confirms that  
391 cohesin-associated loops are significantly shorter in active chromatin (Supp Fig. 4 left). Taken  
392 together, these findings imply that gene and enhancer activity impede cohesin translocation (Fig.  
393 5h).



394  
395  
396

**Fig. 5** Cohesin extrudes further through quiescent regions than active regions. **a** Most CTCF-mediated looping contacts do not reflect the fully extruded state. Estimate is obtained using left

397 TF-protected (start and end at least 15 bp from motif center, length < 115) fragments that overlap  
398 *FactorFinder* identified CBS (+) and have an interaction length greater than 10kb. For each CBS  
399 with at least 50 long-range TF-protected fragments overlapping the motif, % convergent is  
400 calculated as the number of interaction partners overlapping CTCF (-) motifs / total number of  
401 fragments at motif. Because this estimate is conditional on CTCF binding at the anchor, we  
402 divide estimates by two to account for the ~50% occupancy of CTCF<sup>34</sup>. **b** Depiction of how  
403 regions were annotated using ChromHMM. Correlation **(c)** and fragment **(d)** heatmaps for  
404 ChromHMM annotated unique 1 MB regions downstream of left fragments overlapping CTCF  
405 (+) binding sites. All other plots in this figure are filtered to TF-protected (fragment length < 115  
406 bp, start and end at least 15 bp from motif center) fragments. Density **(e)** and P(S) curves **(f)** for  
407 chromatin state clusters shown in **(c,d)**, filtered to the top 20%. Chromatin annotations making  
408 up each cluster are added together and quantiles are obtained to determine fragments in the top  
409 20% of active chromatin, quiescent chromatin, and bivalent / polycomb chromatin. **g** Ridge plots  
410 for the bottom 10% quantile (“Low”) and top 10% quantile (“High”) of H3K27ac bp and number  
411 of RNAPII binding sites. ChIP-seq from ENCODE was used to annotate 1 MB downstream of  
412 left fragments overlapping CBS (+) for this figure. **h** Diagram illustrating differences in  
413 extrusion rates between active and quiescent chromatin states, with numbers obtained from Supp  
414 Fig. 3.

415

## 416 Discussion

417

418 We have developed *FactorFinder*, a transcription factor footprinting method for MNase HiChIP  
419 data and used it to identify CTCF binding sites with near base-pair resolution. We show that the  
420 DNA protection footprints of nucleosomes and transcription factors can be readily distinguished  
421 based on pre-ligation fragment size and strand origin and use these features to identify CTCF  
422 binding sites. Significance is then assessed through a multinomial approach, which avoids  
423 placing distributional assumptions on read counts. Using this method, the median distance  
424 between *FactorFinder* peak summits and motif center is 5 bp, with 93% of peak summits  
425 identified within 20 bp of a CTCF motif center.

426

427 We then leverage this methodological advance to investigate how chromatin state affects cohesin  
428 extrusion dynamics. A close examination of CTCF-protected fragments revealed an additional  
429 CTCF-adjacent footprint downstream of the CBS, which we propose represents cohesin given its  
430 positioning relative to looping orientation as well as its strong association with both long range  
431 interactions and cohesin occupancy. We estimated the frequency with which a CTCF bound  
432 locus forms a loop with a downstream CTCF site and found that it varies considerably from CBS  
433 to CBS, with a genome-wide range from ~1-10%. This is consistent with recent live-cell imaging  
434 work that found that CTCF-mediated loops predominantly exist in the partially extruded state at  
435 two studied loci<sup>13,14</sup>.

436





466 into contact but move away from each other at the time of transcription. Our findings are  
467 compatible with the “kiss and kick” model, but additionally suggest a potential mechanism by  
468 which distal enhancers can locate gene promoters without being stuck in a stable conformation.  
469 This model would use promoter- or enhancer-proximal CTCF sites to enable distal enhancers to  
470 both come into contact with gene promoters and subsequently disengage during transcription. In  
471 this way, CTCF’s role in long-range enhancer promoter contact would be as a dynamic  
472 functional element recruiter instead of mediating continual stable contact between distal  
473 enhancers and gene promoters.

474

## 475 **Materials and methods**

476

### 477 CTCF MNase HiChIP

478 Four MNase K562 CTCF HiChIP (150 bp paired-end) libraries were generated using the Cantata  
479 Bio / Dovetail Genomics MNase HiChIP kit. CTCF MNase HiChIP was performed as described  
480 in the Dovetail HiChIP MNase Kit protocol v.2.0. Briefly, 5 million K562 cells per sample were  
481 crosslinked with 3mM DSG and 1% formaldehyde and digested with 1ul MNase (“YET”  
482 samples) or 2ul MNase (“GW” samples) in 100ul of 1X nuclease digestion buffer. Cells were  
483 lysed with 1X RIPA containing 0.1% SDS, and CTCF ChIP was performed using 1500ng of  
484 chromatin (40-70% mononucleosomes) and 500 ng of CTCF antibody (Cell Signaling, cat #:  
485 3418). Protein A/G beads pull-down, proximity ligation, and library preparation were done  
486 according to the protocol. Libraries were sequenced to a read depth of ~172 million paired end  
487 reads per sample on the Illumina Nextseq 2000 platform.

488

### 489 Software implementation

490 Preprocessing, analysis and figure code used in this paper are available at  
491 [https://github.com/aryeelab/cohesin\\_extrusion\\_reproducibility](https://github.com/aryeelab/cohesin_extrusion_reproducibility). Data figures in this paper were  
492 made in R v.4.1.2 using ggplot.

493

### 494 Data availability

495 Raw and Processed HiChIP data produced in this study will be uploaded to NCBI GEO (GSE  
496 Record ID pending).

497 K562 ChIP-seq RAD21 BED file (Accession ID: ENCFF330SHG), CTCF BED file (Accession  
498 ID: ENCFF736NYC), CTCF bigWig signal value (Accession ID: ENCFF168IFW), RNAPII  
499 BED file (Accession ID: ENCFF355MNE), and H3K27ac BED file (Accession ID:  
500 ENCFF544LXB) were obtained from ENCODE, and CTCF motifs were obtained from the R  
501 package *CTCF*<sup>27</sup> (annotation record: AH104729, documentation:

502 <https://bioconductor.org/packages/release/data/annotation/vignettes/CTCF/inst/doc/CTCF.html>).

503

## 504 **Methods**

## 505 Data Processing

506 4 replicates of K562 MNase CTCF HiChIP data were aligned to the reference genome using the  
507 BWA-MEM algorithm<sup>41</sup>. Ligation events were then recorded using pairtools parse v. 0.3.0<sup>42</sup>,  
508 PCR duplicates were removed, and the final pairs and bam files were generated. HiChIP loop  
509 calls were then made using FitHiChIP Peak to Peak<sup>29</sup> with 2.5kb loop anchor bin size. The  
510 MNase HiChIP processing protocol is based on guidelines from  
511 [https://hichip.readthedocs.io/en/latest/before\\_you\\_begin.html](https://hichip.readthedocs.io/en/latest/before_you_begin.html). Reproducible code is available at  
512 [https://github.com/aryeelab/cohesin\\_extrusion\\_reproducibility](https://github.com/aryeelab/cohesin_extrusion_reproducibility).

513

## 514 Identification of significant motifs

515 We use CTCF motifs identified as significant ( $p < 1e-05$ ) by *FactorFinder* as the set of CTCF  
516 binding sites. This p-value threshold was chosen based on the precision recall curve (Fig. 3b),  
517 and corresponds to a maximum FDR q-value of  $3e-04$ .

518

## 519 Multiple Testing

520 For genome-wide footprinting analysis adjustment for multiple testing, CTCF motifs are  
521 assigned the p-value of the closest *FactorFinder* sliding window. The Benjamini-Hochberg  
522 method<sup>43</sup> was used to obtain q-values.

523

## 524 Estimating cohesin footprints

525 The cohesin footprint is observed by obtaining motif-level coverage estimates +/- 80 bp around  
526 CBS, summing up the coverage across all motifs (within strata), and subtracting the upstream  
527 coverage from the downstream (downstream coverage - upstream coverage) at each base pair.  
528 Note that downstream and upstream are defined relative to the motif strand, so downstream is to  
529 the “left” of CBS (-) and to the “right” of CBS (+) in terms of reference genome base pairs. The  
530 aforementioned strata are defined by RAD21 ChIP-seq signal level (high vs low) and whether  
531 the fragment is the upstream or downstream interaction partner in its pair. RAD21 ChIP-seq high  
532 and low correspond to the top 25% and bottom 25% of ChIP-seq signal value of the adjacent  
533 (within 50 bp of CBS) RAD21 ChIP-seq peak. Note that only mid-size (fragment length between  
534 80 and 120), long range fragments (interaction length > 10kb) are used for this analysis.

535

## 536 Estimating the fully extruded state

537 We estimated a genome-wide range for the fully extruded state by obtaining CTCF/cohesin-  
538 protected upstream fragments overlapping CBS (+) and estimating the fraction of interaction  
539 partners overlapping a downstream convergent negative strand CTCF motif. CBS (+) were  
540 required to have at least 50 CTCF/cohesin-protected upstream fragments overlapping the motif  
541 to enable sufficient sample size for the motif-specific percent convergent calculation. We then  
542 accounted for CTCF occupancy (estimated as ~50%)<sup>34</sup> by dividing this estimate by two. The  
543 point estimate (5%) is the number of interaction partners overlapping a downstream convergent

544 negative strand CTCF motif genome-wide / the total number of fragments genome-wide, and the  
545 range (1-10%) are the 1st and 99th percentile of the CBS-level CTCF-CTCF chromatin loop  
546 estimate.

547

### 548 Determining extruded loop size as a function of chromatin state

549 We used upstream fragments overlapping CTCF binding sites (+) for this analysis. 1 MB regions  
550 downstream of the CBS (+) were annotated using ChromHMM<sup>32</sup> to quantify the percentage of bp  
551 assigned to each of the 15 chromatin states. To simplify annotation, we grouped the 15  
552 chromatin states into three categories (quiescent, polycomb/bivalent, and active) based on their  
553 correlation (Fig 5c). Regions were clustered using Ward's hierarchical clustering method<sup>44</sup> (Fig  
554 5d.). For extrusion dynamics analyses (Fig 5e,f,h), each of the three chromatin categories was  
555 represented by the 20% of regions with the highest fraction of DNA in this state. Extruded loop  
556 size was then estimated as the average log<sub>10</sub> interaction length for each annotation. Only long  
557 range TF-protected fragments (start and end at least 15 bp from the motif center, length < 115,  
558 interaction length > 10kb) were included in this estimate.

559

560 Similarly, high/low H3K27ac corresponds to the top 10% and bottom 10% of the number of  
561 basepairs covered by H3K27ac ChIP-seq peaks in the 1 MB regions downstream of CBS (+).  
562 High/low RNAPII corresponds to the top 10% and bottom 10% of the number of RNAPII ChIP-  
563 seq peaks located in the 1 MB regions downstream of CBS (+). Extruded loop size estimates  
564 were obtained in the same way for these annotated regions; long range TF-protected fragments  
565 were used to estimate the average log<sub>10</sub> interaction length.

566

### 567 Directionality of CBS-adjacent nucleosome position signal

568 Interestingly, the strength of the nucleosome positioning signal is related to the orientation of the  
569 DNA contact. Stratifying nucleosome-bound fragments based on whether they are the upstream  
570 or downstream long-range (>10kb) fragment in a pair (effectively single-cell left or right loop  
571 anchor) produces a differential nucleosome signal inside and outside the loop (Supp Fig. 5). For  
572 both upstream and downstream nucleosome-bound fragments, the nucleosome closest to the  
573 CTCF binding site and inside the loop exhibits a substantially stronger signal than the closest  
574 nucleosome outside the loop. HiChIP ligations are unlikely to fully account for this signal as a  
575 previous study using MNase-seq also showed a directional nucleosome preference around CBS  
576 (see Fig. 1a), although this result was not noted in the text<sup>25</sup>.

577

### 578 **Disclosures**

579

---

580 Dovetail Genomics/Cantata Bio provided reagents and sample processing for HiChIP  
581 experiments. M.B. and M.S.B were employees at Dovetail Genomics during the course of this  
582 research. M.J.A has financial and consulting interests unrelated to this work in SeQure Dx and  
583 Chroma Medicine. M.J.A's interests are reviewed and managed by Dana Farber Cancer Institute.

584 J.K.J. is a co-founder of and has a financial interest in SeQure, Dx, Inc., a company developing  
585 technologies for gene editing target profiling. JKJ also has, or had during the course of this  
586 research, financial interests in several companies developing gene editing technology: Beam  
587 Therapeutics, Blink Therapeutics, Chroma Medicine, Editas Medicine, EpiLogic Therapeutics,  
588 Excelsior Genomics, Hera Biolabs, Monitor Biotechnologies, Nvelop Therapeutics (f/k/a ETx,  
589 Inc.), Pairwise Plants, Poseida Therapeutics, and Verve Therapeutics. J.K.J.'s interests were  
590 reviewed and are managed by Massachusetts General Hospital and Mass General Brigham in  
591 accordance with their conflict of interest policies.

592

## 593 Funding

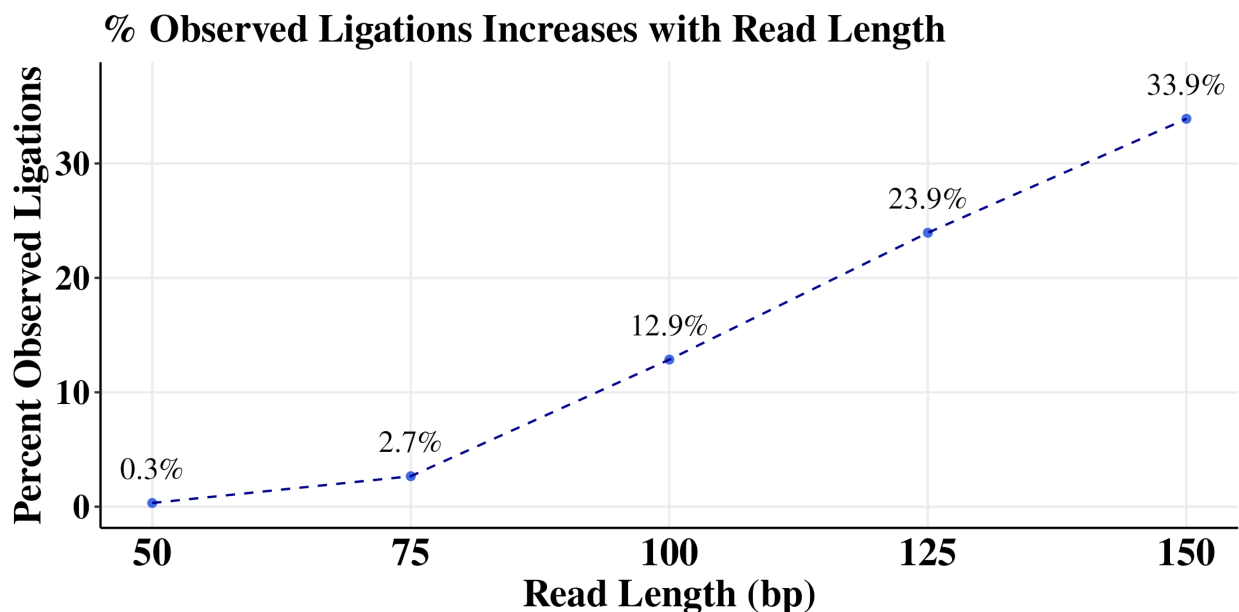
594

595 This work was supported by the National Institutes of Health grants RM1HG009490 (MJA, JKJ,  
596 CS), R35GM118158 (JKJ), T32GM135117 (CS), and a Career Development Award from the  
597 American Society of Gene & Cell Therapy (YET). The content is solely the responsibility of the  
598 authors and does not necessarily represent the official views of the American Society of Gene &  
599 Cell Therapy. Dovetail Genomics / Cantata Bio supported data generation costs.

600

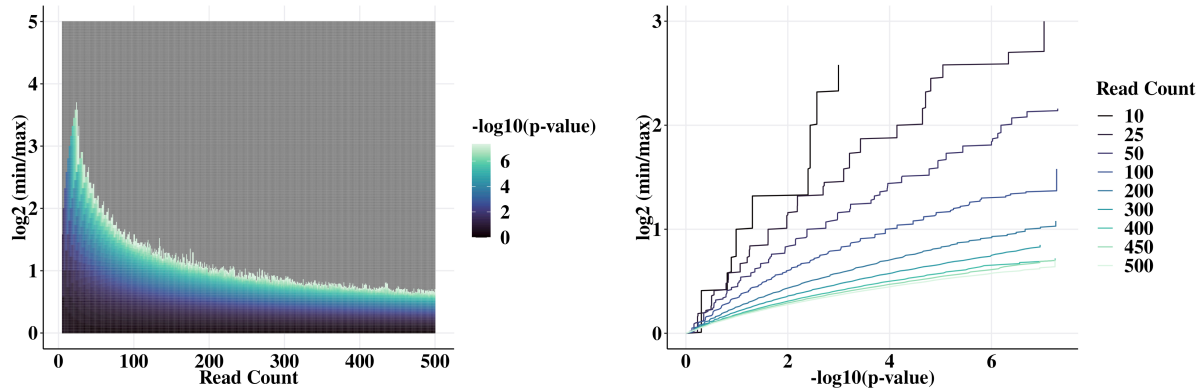
## 601 Supplementary Figures

602



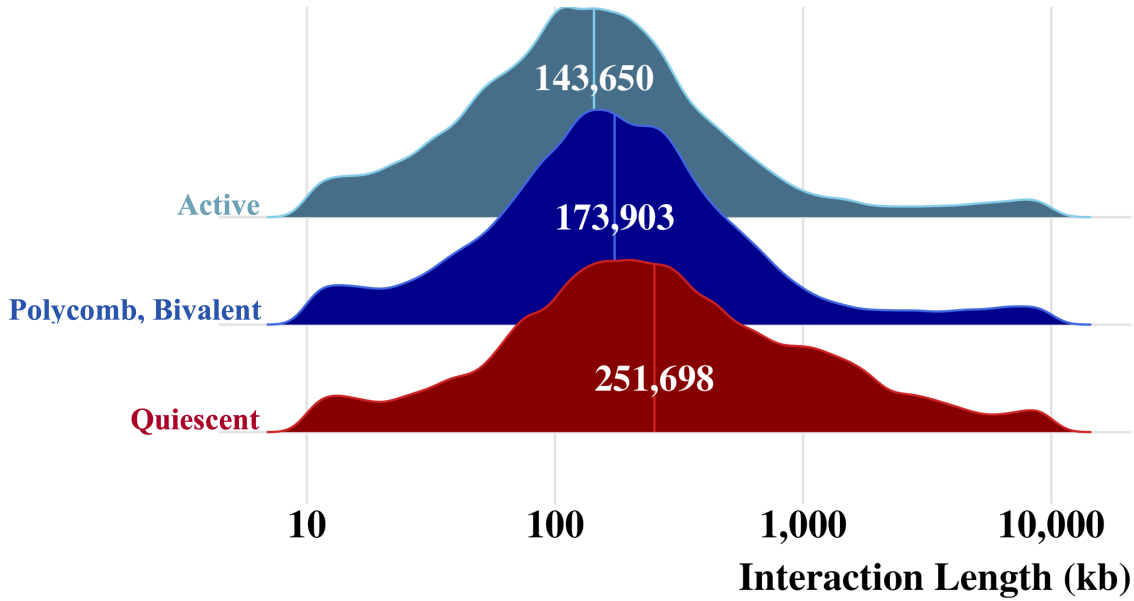
603

604 **Supplementary Figure 1.** Percent observed ligations increases with read length.



605  
606  
607

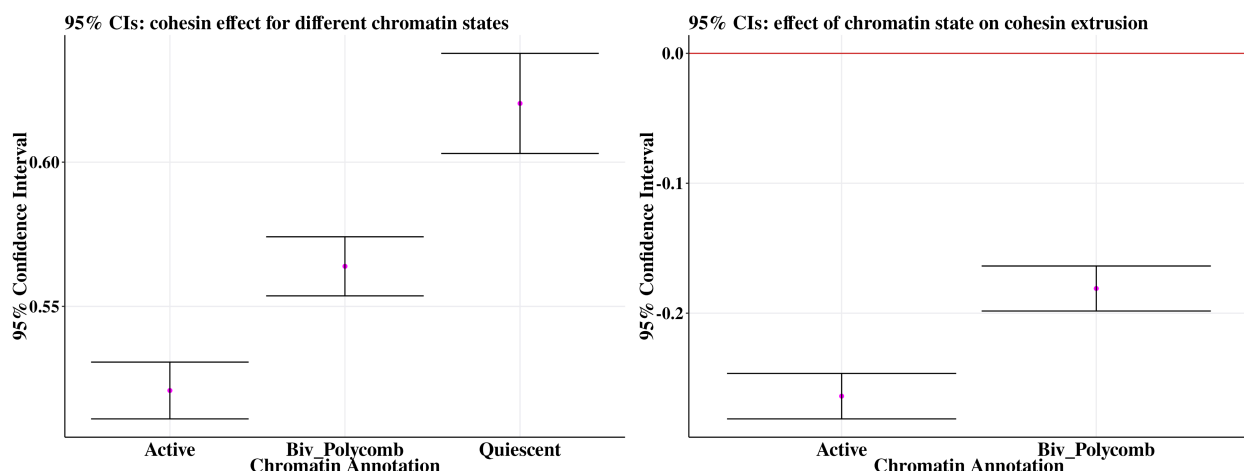
**Supplementary Figure 2.** The probability of observing a high *FactorFinder* statistic under the null hypothesis is higher at low read counts.



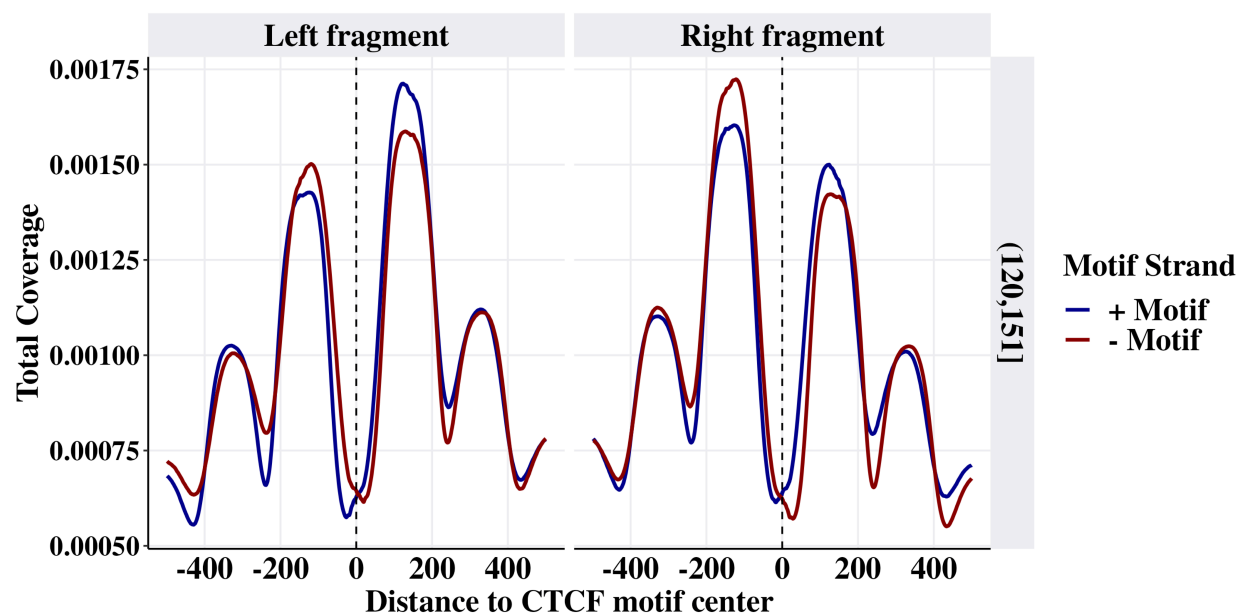
608  
609  
610

**Supplementary Figure 3.** Cohesin extrudes significantly further through quiescent regions than active regions.





611  
612 **Supplementary Figure 4.** Controlling for locus-specific variation with linear mixed models  
613 does not attenuate the relationship between chromatin state and extruded loop size. Note that for  
614 the figure on the right, the group that active and bivalent polycomb are being compared to is  
615 quiescent.



616  
617 **Supplementary Figure 5.** Nucleosomes are preferentially positioned inside the loop.  
618

## 619 References

- 620
- 621 1. Fudenberg, G. *et al.* Formation of Chromosomal Domains by Loop Extrusion. *Cell Rep.* **15**,  
622 2038–2049 (2016).
  - 623 2. Li, Y. *et al.* The structural basis for cohesin–CTCF-anchored loops. *Nature* **578**, 472–476  
624 (2020).
  - 625 3. Xiao, J. Y., Hafner, A. & Boettiger, A. N. How subtle changes in 3D structure can create

- 626 large changes in transcription. *eLife* **10**, e64320.
- 627 4. Zuin, J. *et al.* Nonlinear control of transcription through enhancer–promoter interactions.  
628 *Nature* **604**, 571–577 (2022).
- 629 5. Lupiáñez, D. G. *et al.* Disruptions of Topological Chromatin Domains Cause Pathogenic  
630 Rewiring of Gene-Enhancer Interactions. *Cell* **161**, 1012–1025 (2015).
- 631 6. Flavahan, W. A. *et al.* Insulator dysfunction and oncogene activation in IDH mutant gliomas.  
632 *Nature* **529**, 110–114 (2016).
- 633 7. Hirayama, T., Tarusawa, E., Yoshimura, Y., Galjart, N. & Yagi, T. CTCF Is Required for  
634 Neural Development and Stochastic Expression of Clustered Pcdh Genes in Neurons. *Cell*  
635 *Rep.* **2**, 345–357 (2012).
- 636 8. Katainen, R. *et al.* CTCF/cohesin-binding sites are frequently mutated in cancer. *Nat. Genet.*  
637 **47**, 818–821 (2015).
- 638 9. Kubo, N. *et al.* Promoter-proximal CTCF-binding promotes long-range-enhancer dependent  
639 gene activation. *Nat. Struct. Mol. Biol.* **28**, 152–161 (2021).
- 640 10. Schuijers, J. *et al.* Transcriptional Dysregulation of MYC Reveals Common Enhancer-  
641 Docking Mechanism. *Cell Rep.* **23**, 349–360 (2018).
- 642 11. Cerda-Smith, C. G. *et al.* Integrative PTEN Enhancer Discovery Reveals a New Model of  
643 Enhancer Organization. 2023.09.20.558459 Preprint at  
644 <https://doi.org/10.1101/2023.09.20.558459> (2023).
- 645 12. Davidson, I. F. *et al.* DNA loop extrusion by human cohesin. *Science* **366**, 1338–1345  
646 (2019).
- 647 13. Gabriele, M. *et al.* Dynamics of CTCF- and cohesin-mediated chromatin looping revealed by  
648 live-cell imaging. *Science* **376**, 496–501 (2022).
- 649 14. Mach, P. *et al.* Cohesin and CTCF control the dynamics of chromosome folding. *Nat. Genet.*  
650 **54**, 1907–1918 (2022).
- 651 15. Kasinathan, S., Orsi, G. A., Zentner, G. E., Ahmad, K. & Henikoff, S. High-resolution  
652 mapping of transcription factor binding sites on native chromatin. *Nat. Methods* **11**, 203–209  
653 (2014).
- 654 16. Henikoff, J. G., Belsky, J. A., Krassovsky, K., MacAlpine, D. M. & Henikoff, S. Epigenome  
655 characterization at single base-pair resolution. *Proc. Natl. Acad. Sci.* **108**, 18318–18323  
656 (2011).
- 657 17. Skene, P. J. & Henikoff, S. An efficient targeted nuclease strategy for high-resolution  
658 mapping of DNA binding sites. *eLife* **6**, e21856 (2017).
- 659 18. Gutin, J. *et al.* Fine-Resolution Mapping of TF Binding and Chromatin Interactions. *Cell*  
660 *Rep.* **22**, 2797–2807 (2018).
- 661 19. Hua, P. *et al.* Defining genome architecture at base-pair resolution. *Nature* **595**, 125–129  
662 (2021).
- 663 20. Krietenstein, N. *et al.* Ultrastructural Details of Mammalian Chromosome Architecture. *Mol.*  
664 *Cell* **78**, 554–565.e7 (2020).
- 665 21. Hsieh, T.-H. S. *et al.* Resolving the 3D Landscape of Transcription-Linked Mammalian

- 666 Chromatin Folding. *Mol. Cell* **78**, 539-553.e8 (2020).
- 667 22. Goel, V. Y., Huseyin, M. K. & Hansen, A. S. Region Capture Micro-C reveals coalescence  
668 of enhancers and promoters into nested microcompartments. *Nat. Genet.* 1–9 (2023)  
669 doi:10.1038/s41588-023-01391-1.
- 670 23. Mumbach, M. R. *et al.* HiChIP: efficient and sensitive analysis of protein-directed genome  
671 architecture. *Nat. Methods* **13**, 919–922 (2016).
- 672 24. Chereji, R. V., Bryson, T. D. & Henikoff, S. Quantitative MNase-seq accurately maps  
673 nucleosome occupancy levels. *Genome Biol.* **20**, 198 (2019).
- 674 25. Fu, Y., Sinha, M., Peterson, C. L. & Weng, Z. The Insulator Binding Protein CTCF Positions  
675 20 Nucleosomes around Its Binding Sites across the Human Genome. *PLOS Genet.* **4**,  
676 e1000138 (2008).
- 677 26. Hashimoto, H. *et al.* Structural basis for the versatile and methylation-dependent binding of  
678 CTCF to DNA. *Mol. Cell* **66**, 711-720.e3 (2017).
- 679 27. Dozmorov, M. G. *et al.* CTCF: an R/bioconductor data package of human and mouse CTCF  
680 binding sites. *Bioinforma. Adv.* **2**, vbac097 (2022).
- 681 28. Luo, Y. *et al.* New developments on the Encyclopedia of DNA Elements (ENCODE) data  
682 portal. *Nucleic Acids Res.* **48**, D882–D889 (2020).
- 683 29. Bhattacharyya, S., Chandra, V., Vijayanand, P. & Ay, F. Identification of significant  
684 chromatin contacts from HiChIP data by FitHiChIP. *Nat. Commun.* **10**, 4221 (2019).
- 685 30. Bailey, T. L. STREME: accurate and versatile sequence motif discovery. *Bioinformatics* **37**,  
686 2834–2840 (2021).
- 687 31. Gassler, J. *et al.* A mechanism of cohesin-dependent loop extrusion organizes zygotic  
688 genome architecture. *EMBO J.* **36**, 3600–3618 (2017).
- 689 32. Ernst, J. & Kellis, M. Chromatin-state discovery and genome annotation with ChromHMM.  
690 *Nat. Protoc.* **12**, 2478–2492 (2017).
- 691 33. Hoffman, M. M. *et al.* Integrative annotation of chromatin elements from ENCODE data.  
692 *Nucleic Acids Res.* **41**, 827–841 (2013).
- 693 34. Cattoglio, C. *et al.* Determining cellular CTCF and cohesin abundances to constrain 3D  
694 genome models. *eLife* **8**, e40164 (2019).
- 695 35. Barshad, G. *et al.* RNA polymerase II dynamics shape enhancer–promoter interactions. *Nat.*  
696 *Genet.* 1–11 (2023) doi:10.1038/s41588-023-01442-7.
- 697 36. Banigan, E. J. *et al.* Transcription shapes 3D chromatin organization by interacting with loop  
698 extrusion. *Proc. Natl. Acad. Sci.* **120**, e2210480120 (2023).
- 699 37. Arnold, P. R., Wells, A. D. & Li, X. C. Diversity and Emerging Roles of Enhancer RNA in  
700 Regulation of Gene Expression and Cell Fate. *Front. Cell Dev. Biol.* **7**, (2020).
- 701 38. Transcription decouples estrogen-dependent changes in enhancer-promoter contact  
702 frequencies and spatial proximity | bioRxiv.  
703 <https://www.biorxiv.org/content/10.1101/2023.03.29.534720v2.abstract>.
- 704 39. Benabdallah, N. S. *et al.* Decreased Enhancer-Promoter Proximity Accompanying Enhancer  
705 Activation. *Mol. Cell* **76**, 473-484.e7 (2019).

- 706 40. Pownall, M. E. *et al.* Chromatin expansion microscopy reveals nanoscale organization of  
707 transcription and chromatin. *Science* **381**, 92–100 (2023).
- 708 41. Li, H. & Durbin, R. Fast and accurate short read alignment with Burrows–Wheeler  
709 transform. *Bioinformatics* **25**, 1754–1760 (2009).
- 710 42. Abdennur, N. *et al.* Pairtools: from sequencing data to chromosome contacts. *bioRxiv*  
711 2023.02.13.528389 (2023) doi:10.1101/2023.02.13.528389.
- 712 43. Benjamini, Y. & Hochberg, Y. Controlling the False Discovery Rate: A Practical and  
713 Powerful Approach to Multiple Testing. *J. R. Stat. Soc. Ser. B Methodol.* **57**, 289–300  
714 (1995).
- 715 44. Murtagh, F. & Legendre, P. Ward’s Hierarchical Agglomerative Clustering Method: Which  
716 Algorithms Implement Ward’s Criterion? *J. Classif.* **31**, 274–295 (2014).